Applied Catalysis B: Environmental 220 (2018) 314–323

Contents lists available at ScienceDirect

Applied Catalysis B: Environmental

journal homepage: www.elsevier.com/locate/apcatb

Lignosulfonate-based macro/mesoporous solid protonic acids for acetalization of glycerol to bio-additives

Lakhya Jyoti Konwar[a,*], Ajaikumar Samikannu[a], Päivi Mäki-Arvela[b], Dan Boström[c], Jyri-Pekka Mikkola[a,b]

[a] Technical Chemistry, Department of Chemistry, Chemical-Biological Centre, Umeå University, SE-901 87 Umeå, Sweden
[b] Laboratory of Industrial Chemistry and Reaction Engineering, Johan Gadolin Process Chemistry Centre, Åbo Akademi University, Turku, FI-20500, Finland
[c] Department of Applied Physics and Electronics, Chemical-Biological Centre, Umeå University, SE-901 87 Umeå, Sweden

ARTICLE INFO

Keywords:
Solid sulfonic acids
Glycerol acetalization
Bio-additives
Solketal
Lignosulfonate

ABSTRACT

The enclosed paper introduces a novel, scalable and environmentally benign process for making strongly acidic solid meso/macroporous carbon catalysts from Na-lignosulfonate (LS), a byproduct from sulfite pulping. Ice-templated LS was converted to strongly acidic macro/mesoporous solid protonic acids via mild pyrolysis (350–450 °C) and ion/H^+ exchanging technique. The synthesized materials were extensively characterized by FT-IR, Raman, XRD, XPS, TGA, FE-SEM, TEM and N_2-physisorption methods. These LS derived materials exhibited a macro/mesoporous and highly functionalized heteroatom doped (O, S) carbon structure with large amounts of surface −OH, −COOH and $-SO_3H$ groups similar to the sulfonated carbon materials. Further, these carbon materials showed excellent potential as solid acid catalysts upon acetalization of glycerol with various bio-based aldehydes and ketones (acetone, methyl levulinate and furfural), easily outperforming the commercial acid exchange resins (Amberlite® IR120 and Amberlyst® 70). Most importantly, the optimum LS catalyst exhibiting a large specific surface area demonstrated exceptional potential for continuous solketal production (liquid phase atmospheric pressure operation) maintaining its activity (glycerol conversion ≥ 91%) and structural features even after 90 h time on stream.

1. Introduction

Lignosulfonate or sulfonated lignin (LS) is a side-product from the production of wood pulp through sulfite pulping. Chemically this type of lignins represent a group of water soluble anionic polyelectrolyte polymers recovered from the spent sulfite pulping liquids (black liquor) containing large amounts of sulfonic groups at aliphatic carbons linked via C−S bonds, which roughly translate to 5–6% S in their dry form [1]. During the past few years LS has found wide variety applications in fields such as plasticizers upon concrete manufacture, dispersants in the oil drilling mud, modifiers in polymers, feedstock for producing plasterboard, corrosion inhibitors, flocculants and so on. Even so, in reality the scope of LS in the current market is limited to a handful of applications (cement industry, animal husbandry, mineral processing) and therefore sold in bulk, at low margins. The high level of S renders chemical processing of LS challenging, nonetheless it has been chemically processed into useful products such as dimethyl sulfide, dimethyl sulfoxide and vanillin [2–4]. On the other hand, the presence of naturally occurring $-SO_3Na$ groups make LS an excellent raw material for the synthesis of acidic catalysts and/or acid exchange materials through ion/H^+ exchanging. The concept was recently demonstrated by several researchers, who utilized H^+ exchanged LS as an alternative catalyst for various multicomponent reactions, such as one-pot synthesis of benzoxanthenes by a condensation reaction of dimedone with aldehyde and 2-naphthol and in sugar dehydration [5,6]. Regardless, such H^+ exchanged LS are highly soluble in water and almost all protic solvents; therefore they require a multistep, complicated precipitation and regeneration cycle for reuse. H^+ exchanged LS have also been heterogenized by phenol-formaldehyde type condensation reactions, in which the phenolic −OH groups present in LS are reacted with aldehydes in the presence of an acidic catalyst (usually HCl). These H^+ exchanged phenol-formaldehyde type condensation products of LS have been employed as heterogeneous acid catalysts upon reactions such as hydroxyalkylation/alkylation and saccharification [7,8]. However, irrespective of their excellent properties as an acidic catalyst material, the aforementioned LS or LS based materials have several drawbacks such as poor thermal, mechanical and chemical stability, thus limiting their applicability as a solid catalysts. Also, they do not possess textural

* Corresponding author.
E-mail addresses: lakhya07@gamil.com, klakhyajyoti@yahoo.co.in (L.J. Konwar), jpmikkol@abo.fi (J.-P. Mikkola).

http://dx.doi.org/10.1016/j.apcatb.2017.08.061
Received 5 July 2017; Received in revised form 4 August 2017; Accepted 17 August 2017
Available online 24 August 2017
0926-3373/

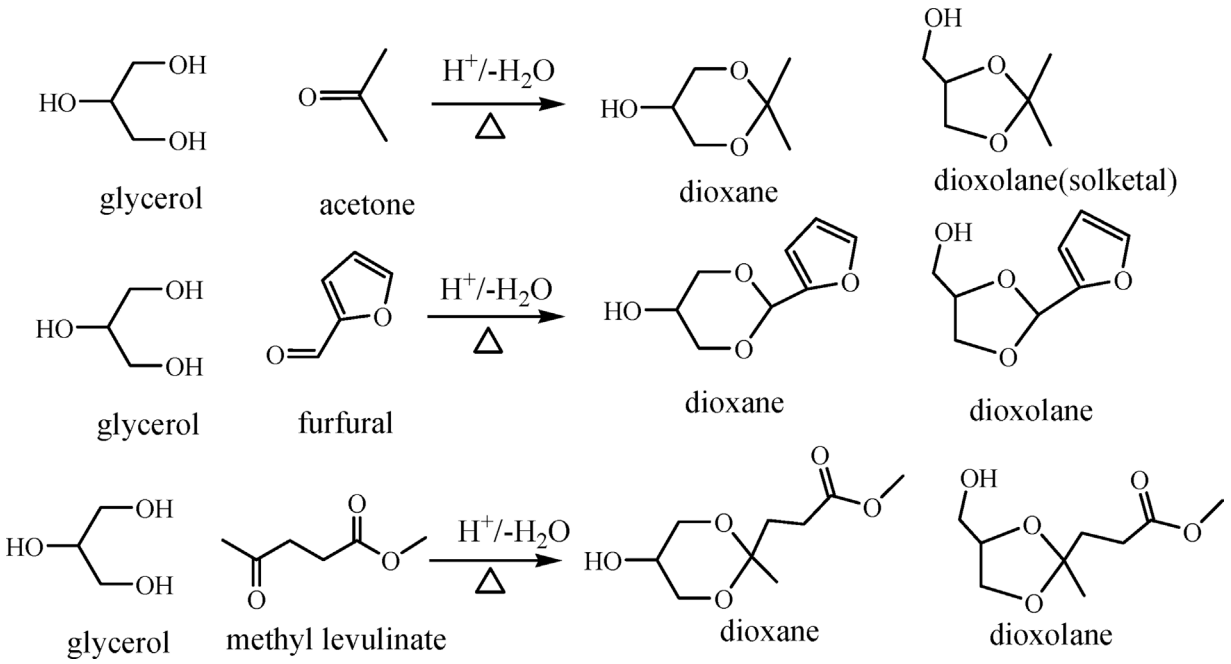

Scheme 1. Reaction scheme for acetalization of glycerol with acetone, furfural and methyl levulinate.

properties of an ideal heterogeneous catalyst such as high specific surface area, well defined porosity etc. Irrespective of this, the potential of LS as a sustainable solid acid catalyst precursor is undeniable. Considering their high carbon content, LS could also serve as an excellent platform for synthesizing versatile carbon materials (e.g. S doped or sulfonated carbon materials) [9].

Glycerol is the main by-product from biodiesel production by transesterification of triglycerides with methanol, corresponding to ca. 10 kg crude glycerol per 100 kg biodiesel produced. The flooding of additional glycerol stemming from biodiesel production into an already saturated market has adversely affected its market value in recent years. Thus, there have been significant efforts to find new applications and processes for glycerol valorization in order to stabilize the glycerol market and also to ensure the sustainability of the biodiesel production [10,11]. The acid catalyzed acetalization of glycerol with aldehydes or ketones is an important reaction for the synthesis of five (dioxolane) and six membered (dioxane) cyclic acetals/ketals (Scheme 1). These products have wide range of industrial applications and have been extensively utilized as solvents, fuel additives, low temperature heat-transfer fluids, surfactants, binders and so forth. In recent years there has been an increasing interest upon the acetalization of glycerol with bio-based carbonyl compounds (furfural, acetone, levulinic acid etc.) which yields renewable bio-additives. Among these, the five membered solketal produced by reacting glycerol with acetone has gained considerable attention as a multicomponent fuel additive in gasoline [12], diesel [13] as well as biodiesel [14] formulations. Solketal synthesis has been investigated over a range of homogeneous as well heterogeneous catalysts including sulfuric acid, *p*-toluenesulfonic acid, aluminosilicates (zeolites, modified SBA-15) [15], mixed oxides (SO_4^{2-}/ZrO_2, supported SnO_2) [16,17], heteropolyacids [18], sulphonic ion exchange resin [19,20] and sulfonated carbons [21].

Among the investigated catalysts, the sulphonic ion exchange resins (Amberlyst® 15 Purolite® PD206, Amberlyst® 36) have been found to be the most efficient and have even been applied in continuous solketal production [22–24]. Nevertheless, these ion exchange catalysts tend to be expensive and are also prone to deactivation (due to H_2O accumulation and leaching) within short periods of time (ca. after 20–24 h on time on stream) [20,22,23]. In addition, most of the reported continuous processes operate at elevated pressures 27–120 bar, leading to increased operational and investment costs [20]. All these factors render the scale-up of an ion exchange resins based process from laboratory to industrial scale difficult. In this regard, LS could be an interesting raw material for the development of an inexpensive and stable heterogeneous catalyst for continuous solketal production.

Keeping the above in mind, the current study was undertaken with the aim of developing a porous, acidic and robust solid catalyst from LS. A novel, environmentally benign method based on ice-templating [25], mild pyrolysis (350–450 °C) and H^+ exchanging of LS was developed; whereby the need of sulfonation step with hazardous sulfonating agents such as conc./fuming H_2SO_4, 4-benzenediazonimsulfonate, $ClHSO_4$ etc.

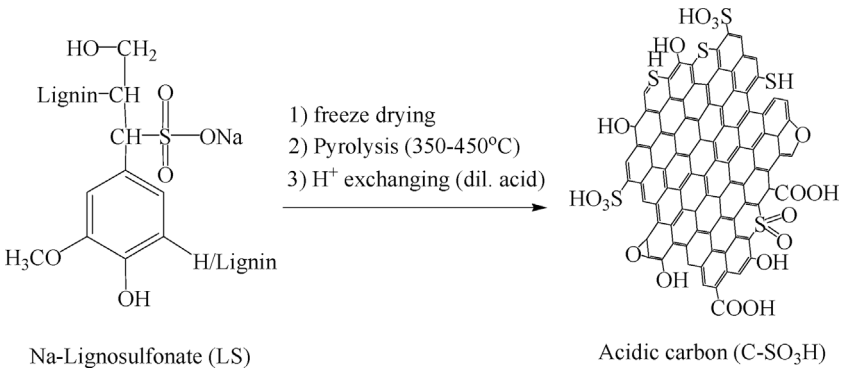

Scheme 2. Method for preparing sulfonic acid functionalized carbon materials from LS.

could be entirely eliminated (Scheme 2) [27–29]. Further, in order to probe the catalytic potential of the synthesized carbon materials acetalization of glycerol with various bio-based aldehydes and ketones was studied in comparison with commercial polymer resins. In addition, glycerol acetalization was investigated in continuous mode (1st study to report fixed bed catalytic application of sulfonated carbons) as well as with furfural and methyl levulinate over such acidic carbon materials for the first time.

2. Experimental

2.1. Materials and methods

Glycerol (99.5%, VWR), anhydrous ethanol (99%, Merck), acetone (99.9%, VWR), furfural (99%, Sigma-Aldrich), methyl levulinate (98%, Sigma-Aldrich), 2,2-dimethyl-1,3-dioxolane-4-methanol or solketal (99%, Sigma-Aldrich), HCl (37%, VWR), NaOH (99%, Sigma-Aldrich), H_2SO_4 (98%, VWR) and Na-polystyrene sulfonate (M.W. 75,000, VWR) were obtained from commercial sources and used without further purification. Na-Lignosulfonate (28% ash, 8% Na, 18% sulfates) was supplied by Aditya Birla Domsjö Fabriker AB pulp mill in Sweden. The polymer resin based catalysts: Amberlyst® 70 (H^+ form, 2.50 mmol/g, $< 1\ m^2/g$, stable up to 200 °C) and Amberlite® IR120 (H^+ form, 1.8 mmol/g, $< 1\ m^2/g$, stable up to 120 °C) were obtained from the Rohm and Haas and Merck, respectively.

2.2. Catalyst preparation

The macro/mesoporous solid sulfonic acids were prepared by a novel ice-templating method, involving mild pyrolysis and acid exchange of ice-templated Na-lignosulfonate (LS) monoliths [25]. In a typical process, ca. 5 g LS was dissolved in mixture of 10 ml deionised water/acetonitrile (3:1, v:v), transferred to a 40 ml freeze dry flasks and submerged in a dry ice/acetone cooling bath (−78 °C) for 30 min. The frozen samples were freeze-dried for ca. 24 h using a CoolSafe Scanvac freeze dryer to give dry LS monoliths. In some instances LS was substituted by 10 and 20% Na-polystyrene sulfonate (PS) (denoted LS-PS monoliths). In the next step, the freeze dried LS or LS-PS monoliths were subjected to mild pyrolysis at temperatures 350–450 °C; the heating rate, holding time and N_2 flow rate were fixed at 30 °C/min, 1 h and 50 ml/min, respectively (Fig. S1, Supporting information). All pyrolysis experiments were performed in a tubular stainless steel reactor, equipped with PID temperature controller, mass flow controller and a SO_2-trap. The solid product from pyrolysis experiments (denoted xLSyPSzNa$^+$, x, y and z represent the percentage of LS, percentage of PS and pyrolysis temperature) were ground to powder and protonated by ion-exchanging with 2 N H_2SO_4 (100 ml acid g^{-1} solid) at room temperature for 24 h. The protonated products (xLSyPSzH$^+$) were filtered and thoroughly washed with a mixture of deionized water and acetone (8:1, v:v) at 80 °C (until the pH of filter liquor was neutral) and dried at 100 °C overnight. For comparison a resin type catalyst (LS-RES) was also prepared by phenol-formaldehyde type condensation reaction between furfural and LS [7,8]. Prior to use the catalyst particles were sieved and particle sizes 10–120 μm collected for further experiments (Fig. S2, Supporting information).

2.3. Catalyst characterization

The carbon materials were characterized by means of Infrared Spectroscopy (Bruker Vertex 80v FT-IR spectrometer with vacuum bench and DTGS detector), Raman spectroscopy (Renishaw InVia laser Raman microscope, 514.5 nm Ar-ion laser), X-ray Powder Diffraction (Bruker-AXS d8 Avance X-ray diffractometer using Cu Kα radiation and Vantec-1 detector) and Thermo Gravimetric Analysis (TGA 4000, PerkinElmer, heated 5 °C/min from ambient to 600 °C under nitrogen flow). The elemental composition and oxidation state of surface functionalities were evaluated by X-ray photoelectron spectroscopy on a Kratos Axis Ultra DLD spectrometer with a monochromatized Al Kα X-ray source operating at 14 kV, 300 W. The analyzer pass energy was 17.9 eV and the energy step was 0.1 eV. The vacuum chamber base pressure was10^{-9} mbar. The morphological features of the carbon materials were studied on a Carl Zeiss Merlin Field Emission Scanning Electron Microscope (FE-SEM) operating at 30 kV. Nitrogen physisorption measurements were conducted on a Micromeritics TriStar 3000 porosimeter. Transmission electron micrographs (TEM) were recorded on a Jeol JEM-2100 electron microscope operating at 200 kV. The resolution was around 0.4 nm. Samples were suspended in ethanol and deposited on a copper grid prior to analysis. Adsorption–desorption isotherms were recorded at −196 °C after the samples were outgassed at 150 °C for 3 h. Specific surface areas were calculated by BET method and pore volumes were calculated from desorption isotherm. Pore size distribution was estimated using the Barrett, Joyner and Halenda (BJH) algorithm (ASAP-2010) available as built-in software from Micromeritics. The amounts of acids groups on the catalyst surface was measured using a titration method as described in previous works [27,28].

2.4. Catalytic tests

2.4.1. Preliminary experiments in batch reactor

Preliminary catalytic tests upon glycerol acetalization with various bio-based carbonyl compounds (acetone, methyl levulinate and furfural) were performed in batch mode using 5 ml Micro-Reaction Vessels, on a heating block equipped with magnetic stirring and nitrogen flow (optional). The reactions were performed with varying amounts of acetone, methyl levulinate and furfural using fixed amount of catalyst (particle size 10–120 μm) in the temperature range of 30–50 °C (acetone) and 100 °C (methyl levulinate and furfural). A steady stream of dry N_2 was also applied when using high boiling methyl levulinate and furfural as acetalizing agent (see below). Upon completed reaction, the quantitative analyses of products were performed by gas chromatography (see below).

2.4.2. Continuous operation

In order to demonstrate the potential of these LS derived materials for large scale catalytic applications, the acetalization of glycerol with acetone was chosen as a reference reaction for the continuous flow study. The reactor was built out of a Pyrex glass tube with an internal diameter of 10 mm and 30 cm length. The reactor column was packed with 0.5 g of powdered LS/LS-PS catalyst (particle size 10–120 μm, bed length 12.5 mm) and it was supported from both ends by 1 mm solid-glass beads (1 g) separated by quartz wool (Fig. 1). The feed containing the reactants glycerol, acetone and anhydrous ethanol solvent (in the mole ratio 6:1:1 or 8:1:1) was continuously pumped into the reactor at different flow rates using an HPLC pump (LKB 2150 HPLC pump), at atmospheric pressure. The reaction was performed at temperatures 30–50 °C (heating was provided with an electrical furnace) and at atmospheric pressure. At the system exit, samples were taken at 60 min intervals and analyzed by gas chromatography.

2.5. Product analysis

The products from acetalization reactions were diluted with acetonitrile and analyzed on a GC-FID (Agilent 6890 N) equipped with a HP-INNOWax column (30 m length, 0.25 mm internal diamter, and 1 μm of film thickness). Helium was used as the carrier gas. The GC injection port and the detector temperature were set at 250 °C. The following temperature program was used for the analysis: initial column temperature was set at 100 °C for 1 min and programmed from 100 °C to 210 °C with the rate of 10 °C min^{-1} and held at this temperature for 10 min. Glycerol conversion and solketal quantification were based on calibration curves obtained with standard compounds.

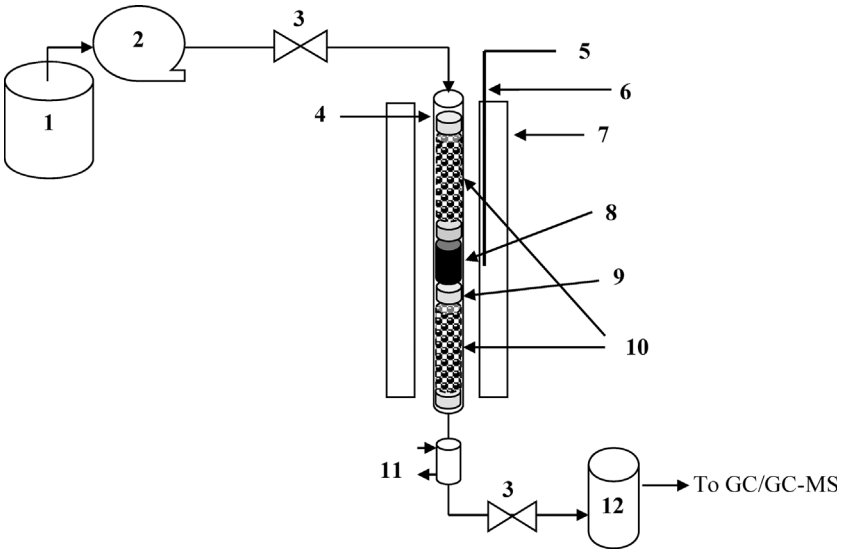

Fig. 1. Experimental set-up for continuous acetalization of glycerol to solketal. 1. Feed vessel (glycerol acetone mixture), 2. HPLC pump, 3. On–off valve, 4. Reactor, 5. Temperature controller, 6. Thermocouple, 7. Furnace, 8. Catalyst bed, 9. Quartz wool support, 10. 1 mm glass beads, 11. Cooling jacket, 12. Product collection vessel.

The products from acetalization of methyl levulinate and furfural with glycerol were quantified by GC–MS (Agilent technologies model 5579N) equipped with HP-5MS capillary column (30 m length, 0.25 mm internal diameter, 0.25 μm film thickness). The glycerol conversion and product selectivity are defined as follows:

$$\text{Conversion}\ (\%) = \frac{C_0 - C_t}{C_0} \times 100 \quad (1)$$

$$\text{Selectivity}\ (\%) = \frac{C_{product}}{C_0 - C_t} \times 100 \quad (2)$$

Where, c_o and c_t represent the initial and final concentration of glycerol, respectively while $c_{product}$ denotes the concentration of acetal/ketal product formed in mol/L. The catalyst turnover frequencies (TOF) were calculated using according to the equation below.

$$TOF = \frac{k \times C_o}{n} \quad (3)$$

where C_o denotes the amount of glycerol (in mmol) loaded into the reactor and n is the amount of active/strong acid sites on the catalyst loaded into the reactor.

3. Results and discussion

3.1. Catalyst characterization results

3.1.1. FT-IR results

Fig. 2 shows the FT-IR patterns of various xLSyPSzH$^+$'s samples obtained from LS/LS-PS monoliths at different pyrolysis temperatures in comparison to untreated LS (Na-lignosulfonate). All pyrolyzed samples exhibited the typical bands of $-SO_3H$ functionalized semi-carbonised materials: 1580 cm^{-1} (aromatic C=C), 1700 cm^{-1} (C–O, C=O), 3500 cm^{-1} (S–OH stretching), 1033 cm^{-1} and 1008 cm^{-1} (S=O symmetric stretching), 1175 cm^{-1} and 1240 cm^{-1} (asymmetric SO_2 stretching) [26–29]. Also, the more prominent S=O symmetric stretching and asymmetric SO_2 observed for LS-PS derived samples suggest the positive impact of PS substitution upon $-SO_3H$ density of carbon materials. In contrast, for neat LS consisting of $NaSO_3H$ groups the corresponding S=O symmetric stretching and asymmetric SO_2 stretching peaks appeared at 997 cm^{-1}/1039 cm^{-1} and 1140 cm^{-1}/1215 cm^{-1}, respectively. The carbonized samples also exhibited the typical bands of carbonyl groups (C=O, C–O, near 1700 cm^{-1}), aromatic C–H stretching (near 2900 cm^{-1}) and characteristic peaks of incompletely carbonised materials near 1580 cm^{-1} (attributable to C=C aromatic ring modes) with varied absorbance. Same peaks were also observed for untreated LS along with a strong –OH band near 3360 cm^{-1} consistent with a phenolic/lignin back bone with –COOH, C–O, $-SO_3H$ like functional groups [5].

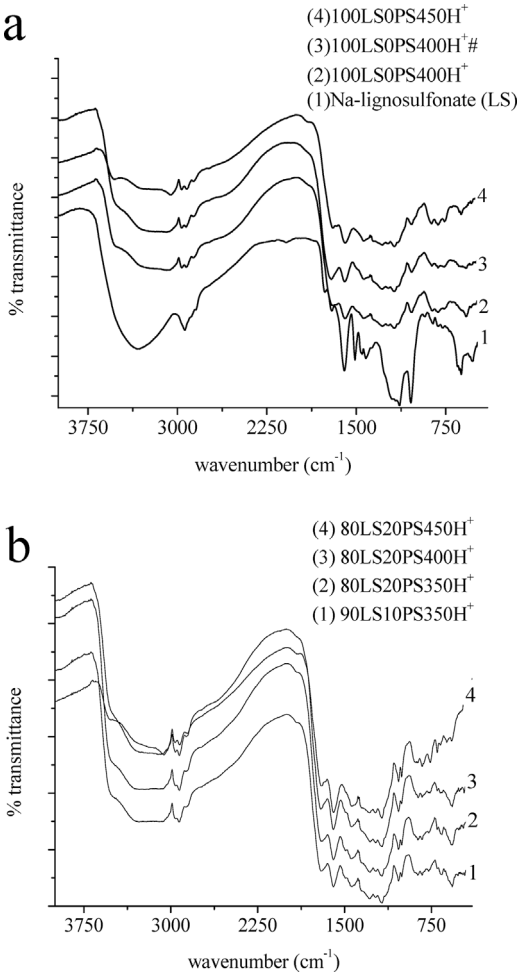

Fig. 2. FT-IR spectra of various (a) LS and (b) LS-PS monolith derived carbon samples obtained under different conditions.

3.1.2. XRD results

The untreated LS samples exhibited a broad peak near 2θ = 15–30°

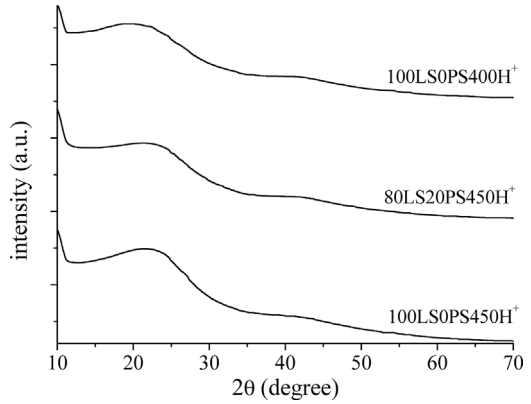

Fig. 3. XRD pattern of selected carbon samples obtained from LS/LS-PS monoliths.

which was associated with the lignin backbone, while several sharp peaks appearing at 2θ = 22.2°, 23.2°, 25.3°, 31.5° and 33.6° could be assigned to the inorganic $NaSO_3R$ species (Fig. S3, Supporting information) [5,30]. In contrast, the pyrolyzed, H^+ exchanded LS/LS-PS samples exhibited XRD patterns consistent with semi-carbonised or amorphous carbon materials, a broad (002) diffraction peak near 2θ = 15–30° and a very weak (101) graphitic structure peak near 2θ = 35–50°, corresponding to a carbon structure comprised of highly functionalized and randomly oriented polycyclic aromatic carbon sheets (Fig. 3) [26,28,31]. The amorphous structure of xLSyPSzH$^+$'s samples were also supported by the findings of laser Raman studies with all samples exhibiting the D-(disordered) and G-(graphitic) bands (Fig. S4, Supporting information) with I_D/I_G intensity ratio ≥ 0.78 (Table 1), consistent with a disordered and amorphous carbon structure [26,29].

3.1.3. XPS results

Fig. 4 shows a representative XPS spectrum for 80LS20PS450H$^+$ sample showing the characteristic signals of C, S, and O elements. All samples showed a prominent C1s peaks around 284.8 and 286.1 eV associated with various C—C, C═C and C—S, C—S bonds of amorphous carbon structure. While the S2p and S2s peaks at 164, 169.1 and 233 eV could be assigned to S—H, S—O and S═O bonds, confirming the presence of functionalized sulfonic groups on all the LS/LS-PS derived carbon samples [30–34]. In such sulfonated materials, the S2p

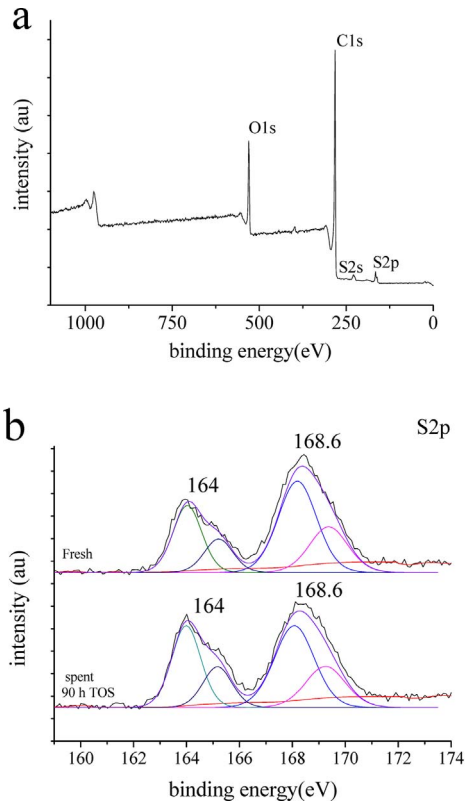

Fig. 4. XPS measurement showing the (a) survey, (b) S2p spectra over the 80LS20PS450H$^+$ sample.

photoelectron peak (163–168 eV) is of particular significance and has been used to verify the presence of the active/strongly acidic $-SO_3H$ groups [28,30–34]. Herein, the LS/LS-PS monolith derived carbon material exhibited the characteristic peaks of both reduced (R—S, —SH, C═S and elemental S) and oxidised ($-SO_3H$) S species, where the ratio of oxidised/reduced S varied as a function of carbonization temperature and composition of monolith precursor (Table 2).

Further, in the current study, the concentration of $-SO_3H$ species on carbonized products was found to decrease with increasing pyrolysis/carbonization temperature, which was probably associated with the

Table 1
Surface and textural characteristics of the carbon materials obtained from LS/LS-PS monolith.

Catalyst	[a]S_{BET} (m^2/g)	[b]V_p (cm^3/g)	[c]D_p (nm)	[d]V_{mp}(cm^3/g)	I_D/I_G	[e]SO_3H (mmol/g)	[f]acid density (mmol H^+/g)
LS (Na form)	< 1	–	–	–	n.d	2.61	n.d
LS-RES	3	0.023	18.5	0	n.d	2.08	n.d
Amberlyst® 70	< 1	–	–	–	n.d	2.50	2.50
Amberlite® IR120	< 1	–	–	–	n.d	1.80	1.80
100LS0PS350H$^+$	2	0.018	47	0	0.90	1.09	4.2
100LS0PS400H$^+$	6.5	0.019	14	0	0.87	0.84	3.7
100LS0PS400H$^+$[g]	10	0.043	18	0	n.d	0.58	3.94
100LS0PS450H$^+$	12	0.033	14.3	0.0007	0.84	0.32	2.99
90LS10PS350H$^+$	4	0.019	21	0	n.d	1.24	4.74
90LS10PS450H$^+$	35	0.14	13.3	0.001	0.84	n.d	3.1
80LS20PS350H$^+$	11	0.019	14	0	0.85	n.d	5.0
80LS20PS450H$^+$	122	0.32	14.5	0.024	0.80	1.21	3.49
80LS20PS450H$^+$[h]	95	0.20	12	0.013	n.d	1.18	3.48

[a] specific surface area.
[b] total pore volume at P/P_0 = 0.95.
[c] average pore diameter.
[d] micropore volume.
[e] based on XPS/elemental analysis (excluding% of S—H and C═S).
[f] total acidity based on titration.
[g] treated with 50% H_2O_2 at 60 °C for 6 h.
[h] After 90 h time on stream.

Table 2
Elemental composition of LS and LS/LS-PS monolith derived carbon samples.

Catalyst	C (at%)	O (at%)	S (at%)	Na (at%)	[a]S2p (BE/eV)		
LS (Na form)	62.5	28.24	3.84	4.25	164.0 (10%),	–	168.3 (90%)
100LS0PS350H$^+$	79.31	18.74	1.95	–	164.0 (36.4%),	165.8 (6.7%),	168.3 (54.7%)
100LS0PS400H$^+$	84.23	14.04	1.71	–	164.0 (46.1%),	165.8 (11.5%),	168.3 (42.3%)
100LS0PS400H$^+$[b]	81.9	16.81	1.3	–	164.0 (55.5%),	–	168.3 (44.5%)
100LS0PS450H$^+$	84.9	13.56	1.54	–	164.0 (60%),	165.8 (8.8%),	168.3 (30.2%)
90LS10PS350H$^+$	84.64	12.50	2.86	–	164.0 (43.7%),	165.8 (5%),	168.3 (51.3%)
80LS20PS450H$^+$	84.8	12.68	2.53	–	164.0 (35.1%),	–	168.3 (64.9%)
80LS20PS450H$^+$[c]	84.74	12.73	2.53	–	164.0 (37.1%),	–	168.3 (62.9%)

[a] Relative proportions of components in parentheses.
[b] treated with 50% H_2O_2 at 60 °C for 6 h.
[c] After 90 h time on stream.

carbothermal reduction of lignin–$NaSO_3$ and/or polystyrene–$NaSO_3$ groups to Na_2S, R—SH and/or aromatic S like species [29–32]. This was also evident from the S2p photoelectron peaks of the untreated and pyrolyzed LS monoliths, with the former exhibiting all of S species (ca. 90%) in the oxidized $-SO_3H/SO_3Na$ form (Fig. S5, Supporting information). The inorganic Na_2S_x species could be removed upon acid washing (H^+ exchanging step) which in part also contributed to the development of the meso/macroporosity (recognized by a strong sulfurous 'rotten egg' odour, i.e. H_2S release, $Na_2S_x + 2H^+ = (x-1)S + H_2S + 2Na^+$), even so the post acid washed samples still exhibited a strong S2p photoelectron peak near 164 eV which most likely corresponds to aromatic/heterocyclic S species, in some cases a new S2p photoelectron peak near 165.8 eV was also detected which correspond to C=S and further confirmed the existence of heterocyclic S bonds within the carbon framework (Table 2) [30,33]. An attempt to increase the concentration of $-SO_3H$ species on a representative carbon sample by H_2O_2 oxidation was ineffective, also supporting the formation of aromatic/heterocyclic S structures during carbonization/pyrolysis step (Table 2).

3.1.4. TGA results

In terms of operational stability, sulfonic acid functionalized carbon materials usually exhibit limited thermal stability of C—SO_3H bonds and the stability of the materials reported herein also followed the trend previously observed for sulfonated carbon materials [28,31,34]. A representative TGA profile of 80LS20PS450H$^+$ sample taken under N_2 flow is shown in Fig. 5. The 1st rapid weight loss region that occurred between 25 and 100 °C corresponds to the loss of moisture and adsorbed gases while the 2nd region between ca. 230–450 °C related to the removal of $-SO_3H$ groups and carbonization, similar to the classical sulfonated carbons obtained by two step carbonization and sulfonation methods [26,28,31,34]. This corresponds to an operational stability close to 230 °C, outperforming even the most stable commercial acidic ion-exchange resin Amberlyst®70. In contrast, neat LS showed a continuous weight loss pattern starting from 60 °C to 730 °C with varying rates; the most rapid weight loss occurred between 180 and 615 °C which corresponds to removal of surface functional groups and carbonization steps (release of SO_3, SO_2, CO, CO_2 etc.). This shows the usefulness of pyrolysis/carbonization as effective method for increasing the degree of crosslinking of LS, improving its heterogeneity and reducing its solubility in various media (H_2O, alcohol etc.).

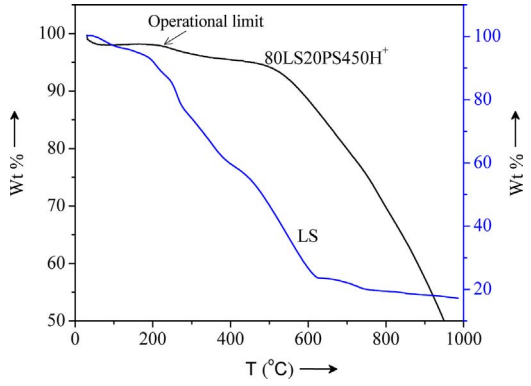

Fig. 5. A representative TGA pattern showing the thermal stability of 80LS20PS450H$^+$ sample.

3.1.5. Nitrogen physisorption and acidity measurement results

The specific surface area, pore size, pore volume and surface acidities of the different xLSyPSzH$^+$'s samples obtained from freeze-dried LS and LS-PS monoliths are given in Table 1. These results are consistent with effects of pyrolysis/carbonization conditions and composition of LS monoliths on the acidic and textural properties of the prepared carbon samples. The decreased acidity and increased porosity with increasing pyrolysis temperature are in agreement with XPS results (see above), and similar to the trends reported for pyrolysis of ice-templated PS monoliths [30]. Herein, the carbon samples obtained at pyrolysis temperature of 350 °C were essentially non-porous/macroporous (BET specific surface area 1–5 m^2/g), while those obtained at 450 °C exhibited reasonable porosity with BET specific surface areas between 35 and 122 m^2/g. In contrast, the samples obtained without ice-templeting/freeze drying step which non-porous (BET specific surface area < 1 m^2/g) even after pyrolyzing at temperatures reaching 500 °C (data not shown).

Furthermore, substitution/addition of PS in the LS monoliths was found to have a positive impact on the $-SO_3H$ density and porosity development as it led to an increase in the overall $NaSO_3$ content of the monolith samples. The PS substitution also helped in preserving the ice-templated porous structure by promoting intermolecular crosslinking during pyrolysis which led to more porous products/catalysts [30]. Here, the carbon samples obtained at 450 °C exhibited a mixed meso/macroporous structure with average pore diameters between 14 and 17 nm and reasonably high specific surface areas (BET ≥ 35 m^2/g). Overall, the 80LS20PS450H$^+$ sample, obtained from freeze-dried LS-PS monoliths (containing 20 wt% PS) at 450 °C, exhibited the highest BET specific surface area of 122 m^2/g. These results are significant improvement over the previously reported resin type catalysts based on LS [7,8].

From the acidity measurement results complied in Table 2, we can see that these carbon materials exhibit acidity (total acidity) in the range of 2.99–5.0 mmol/g. The acidity values are 1.6–2.7 times and 1.2–2.0 times higher than Amberlite® IR120 (H^+) and Amberlyst® 70 (H^+), respectively. However, unlike the polymer resins, the total acidity of carbon materials was not representative in terms of the concentration of catalytically active strong or $-SO_3H$ sites as these values also include acidity contributions from weakly acidic —COOH and —OH groups. On the contrary, the $-SO_3H$ density of the prepared carbon materials was significantly lower (1.4–3.1 times and 2–4 times

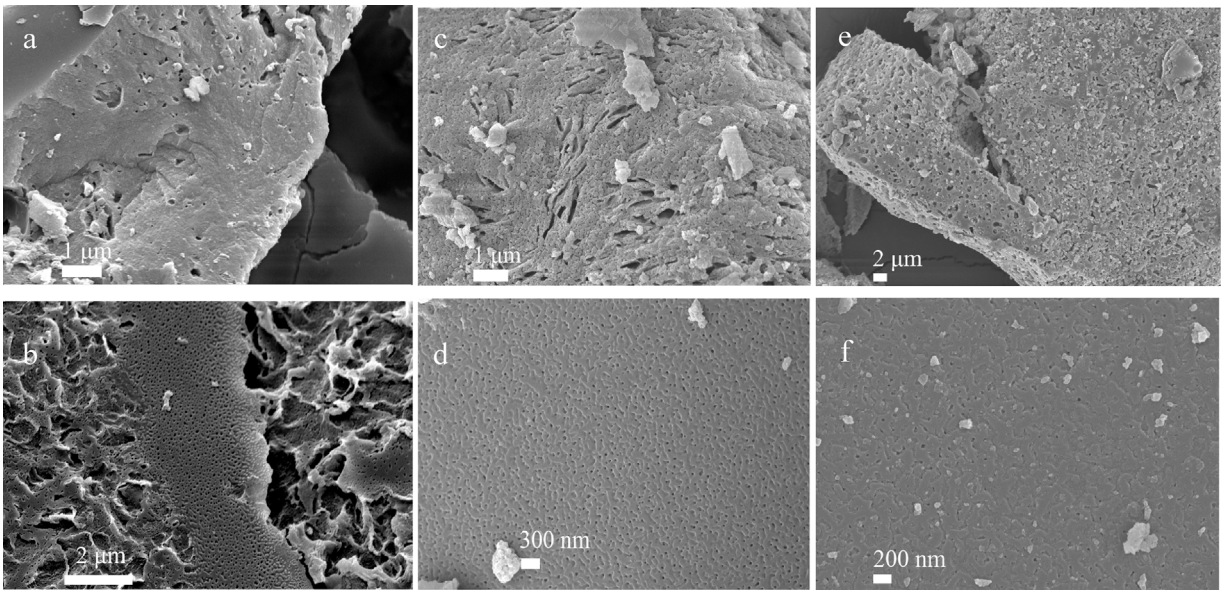

Fig. 6. FE-SEM images of representative carbon samples (a) 100LS0PS450H$^+$ (1 µm), (b) 90LS10PS450H$^+$ (2 µm), (c) 80LS20PS450H$^+$ (1 µm), (d) 80LS20PS450H$^+$ (300 nm), (e) 80LS20PS450H$^+$ 90 h after time on stream (2 µm) and (f) 80LS20PS450H$^+$ after 90 h time on stream (200 nm).

lower than that of Amberlite® IR120 and Amberlyst® 70). Even so, the reported carbon materials demonstrated catalytic activity which was *on par* the best polymer resins (see below) [19,22,23].

3.1.6. FE-SEM and TEM results

Further confirmation of the hypothesis regarding the effects of PS substitution on porosity development was supported by SEM analysis of the carbon samples. As can be seen in the FE-SEM images presented in Fig. 6, the carbo-catalyst samples obtained from neat LS monoliths at 450 °C (100LS0PS450H$^+$) clearly exhibited less porous/dominantly macroporous topography with no visible mesopores whereas those obtained from the LS-PS monoliths under identical conditions demonstrated well-defined and uniform macro and mesopores (80LS20PS450H$^+$ and 90LS10PS450H$^+$).

Further investigation of the 80LS20PS450H$^+$ sample by TEM analysis also reveal a porous and non-uniform surface structure. The textured surface morphology with randomly arranged aromatic carbon sheets and well developed mesopores observed in Fig. 7 was in agreement with N_2 physisorption results and comparable to the porous sulfonated carbons reported in our earlier works [28,34]. Most importantly, the porous morphology could be maintained even after continuous catalytic operation in liquid phase reaction (90 h time on stream) (Fig. 7(b)).

To summarize our results, it can be concluded that the ice-templated LS/LS-PS monolith derived semi-carbonised materials exhibit a porous and highly functionalized heteroatom doped (O, S) carbon structure with large amounts of surface −OH, −COOH and −SO_3H groups which closely resemble the sulfonated or sulfonic acid functionalized carbon materials [26,28,31].

3.2. Catalytic activity

3.2.1. Batch experiment results

In order to probe the catalytic potential of the LS/LS-PS derived functional carbon materials as a Brønsted acidic catalyst preliminary catalytic tests conducted upon glycerol acetalization with acetone in batch mode. Fig. 8(a) shows the results of catalytic activity testes as a function catalyst TOF, the plots in Fig. 8(a) clearly demonstrate the superiority of LS/LS-PS derived carbo-catalysts over commercial polymer resins and LS-RES, a resin type catalyst obtained by H^+ exchanging condensation product of LS and furfural [7,8]. Further, the TOFs among the prepared LS/LS-PS carbo-catalysts followed a trend that was consistent the effect of acid site density and porosity. Overall, the carbo-catalyst 80LS20PS450H$^+$, corresponding the highest porosity (122 m^2/g, 0.32 cm^3/g) and a high −SO_3H density (1.21 mmol/g) exhibited highest catalytic activity. Subsequently, the 80LS20PS450H$^+$ catalyst was chosen for further optimization of reaction parameters. Fig. 8(b)–(d) summarizes the effects of reaction temperature, acetone-to-glycerol mole ratio and reuse (operational stability). The trends of glycerol conversion vs. reaction temperature studied at 6:1 mol ratio show the positive influence of increased reaction temperature on initial rate of reaction, however temperature was found to have negative effect

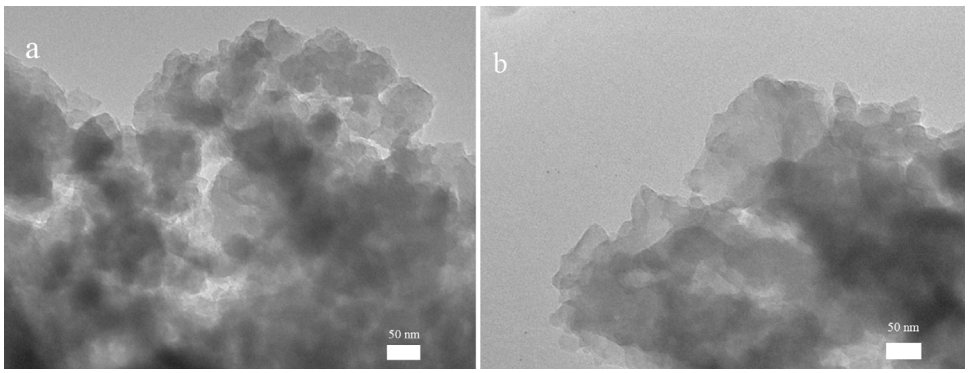

Fig. 7. TEM images of a representative carbon samples 80LS20PS450H$^+$ (a) fresh and (b) after 90 h time on stream (scale bars: 50 nm).

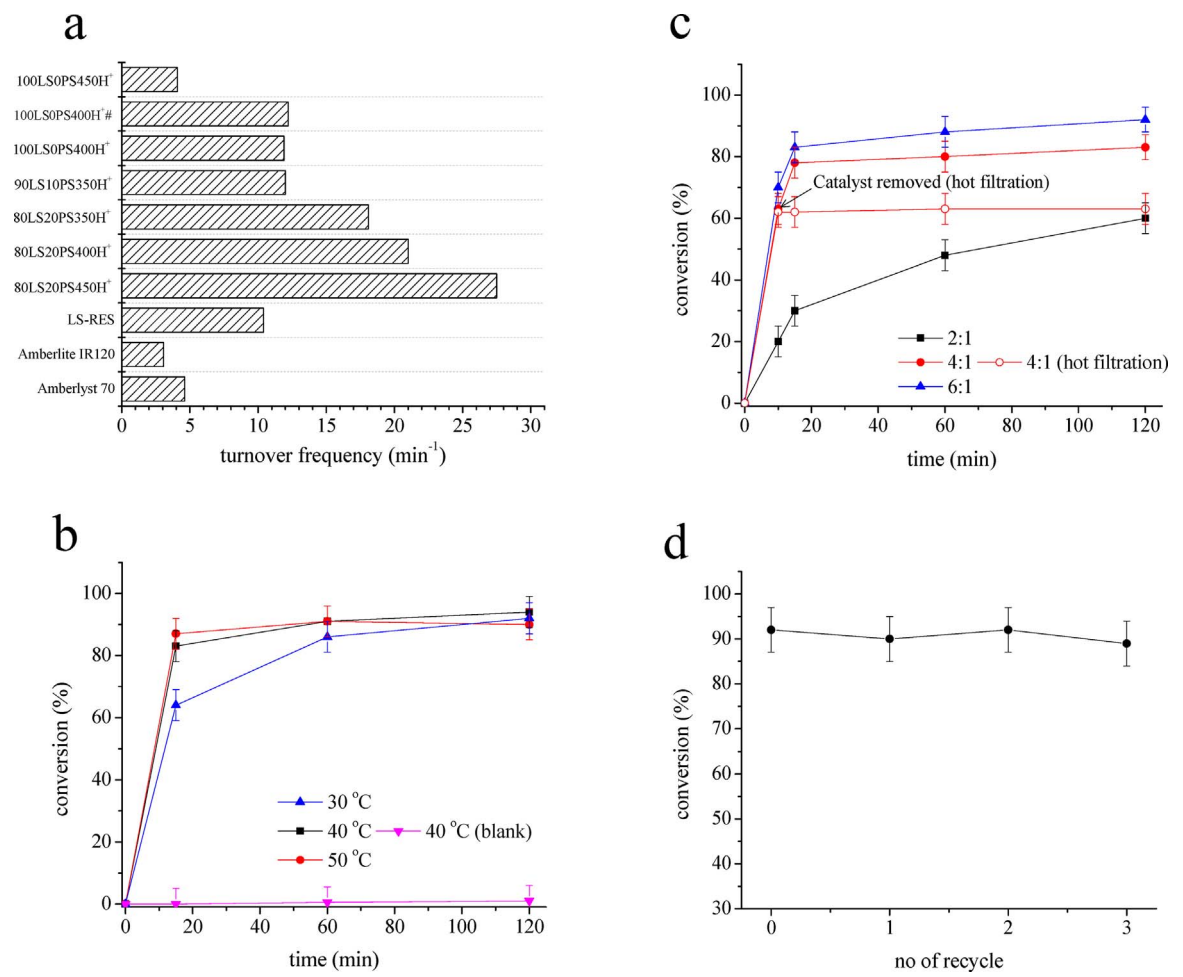

Fig. 8. (a) TOF as a function of catalyst (conditions: acetone/glycerol = 6, T = 50 °C, 300 rpm), (b) glycerol conversion as a function of reaction temperature and (conditions: 5 wt% 80LS20PS450H$^+$, acetone/glycerol = 6, 300 rpm) (c) glycerol conversion as a function of acetone to glycerol mole ratio (conditions: 5 wt% 80LS20PS450H$^+$, T = 40 °C, 300 rpm) (d) glycerol conversion as a function of reuse (conditions: 5 wt% 80LS20PS450H$^+$, acetone/glycerol = 6, T = 40 °C, t = 60 min, 300 rpm); solketal selectivity was ≥99.5% in all cases.

on the final reaction equilibrium, the reduced conversion at 50 °C (ca.90%) was consistent with the exothermic nature of the reaction (Fig. 8(a)) [19]. The requirement of stoichiometric excess acetone and increasing trend of glycerol conversion observed with increasing acetone amount (practical conversions could only be achieved at acetone-to-glycerol mole ratios of 6:1) was in good agreement literature results and the thermodynamically driven reaction equilibrium (Fig. 8(b)) [17–23]. It is also worth mentioning here that irrespective of the catalyst type or reaction conditions the 5-membered dioxolane (solketal) was formed exclusively (selectivity > 99.5%). The heterogeneous nature and stability of catalyst active sites were experimentally confirmed by hot filtration tests, whereupon glycerol conversion didn't increase after removal of catalyst from reaction mixture by hot filtration (Fig. 8(c)). Further, the 80LS20PS450H$^+$ catalyst also demonstrated exceptional operational stability and maintained its catalytic activity upon multiple reaction cycles which could be attributed to its high specific surface area stable active (−SO_3H) sites (Fig. 8(d)). Overall, under optimized reaction conditions 94% glycerol conversion and 99.5% solketal selectivity was achieved which was *on par* to the activity of the best sulphonic ion-exchange resins [19,20].

Encouraged by these results, 80LS20PS450H$^+$ catalyst was further evaluated upon glycerol acetalization with furfural and methyl levulinate as carbonyl compounds under solvent free conditions (Table 3). The reaction conditions were selected on the basis of previous studies [35,36]. The formation of condensation products was favored upon use of excess carbonyl compound, continuous H_2O removal (with N_2 purging) or both, characterizing the thermodynamically controlled reaction equilibrium. However, from the prospective of realistic application, use of a lower amount of carbonyl compound and continuous H_2O removal (N_2 purging) are desirable as the high boiling points of furfural (161 °C) and methyl levulinate (193–195 °C) would render the downstream product separation and purification expensive (Table 3) [37]. With the use of equimolar amounts of reactants, glycerol

Table 3
Results of batch catalytic tests conducted upon acetalization of glycerol with furfural and methyl levulinate.

Carbonyl compound	Carbonyl compound/ glycerol (mole ratio)	Time (min)	Glycerol conversion (%)	Selectiveity (%)	
				dioxolane (5 membered ring)	dioxane (6 membered ring)
Furfural	4[a]	120	80	52	48
	4	60	100	51	49
	2	60	93	51	49
	1	60	63	51	49
Methyl levulinate	4	60	100	53	47
	2	60	97	53	47
	1	60	67	52	48

Reaction conditions: 0.5 wt% catalyst, 100 °C with 50 ml/min N_2 flow, 300 rpm stirring rate.
[a] N_2 flow was stopped.

conversion reached only 63% and 67% in 60 min for furfural and methyl levulinate, respectively. In contrast, glycerol conversion was upto 95% in 60 min for furfural condensation with two-fold excess of furfural while, in case of methyl levulinate, glycerol conversion was 97% under identical reaction conditions. Complete conversion was obtained with the use of four fold excess of carbonyl compound. Also, when N_2 purging was not applied, the reaction proceeded much slower, resulting in only 80% glycerol conversion in 120 min with furfural as the acetalizing agent.

However, unlike acetone, the reaction with furfural and methyl levulinate produced a mixture of 6-membered (dioxane) and 5-membered ketal/acetal (dioxolane) compounds (Fig. S6, Supporting information). In case of furfural, the selectivity to dioxolane and dioxane were 52–51% and 49–48%, respectively. In case of methyl levulinate, the selectivity to dioxane was 48–47% and to dioxolane 53–52%, respectively. Overall, these results obtained with the best LS catalyst were superior to several catalysts reported for furfural glycerol condensation reported in previous works, including montmorillonite K-10 (79% glycerol conversion in 2 h at 100 °C using 5 fold excess furfural), Al-MCM-41 (84% glycerol conversion in in 2 h at 100 °C using 5 fold excess furfural) and Al-SBA-15 (74% in 12 h at 100 °C using 1.5 fold excess furfural) [35,36]. Meanwhile, glycerol acetalization with methyl levulinate has not been previously investigated over solid catalysts and the results summarized in Table 3 represent the best results obtained over solid acid catalysts [38].

3.2.2. Results from continuous operations

The acetalization product solketal is a material with excellent market opportunities and has been considered as a potential additive in various fuel formulations (gasoline, diesel and biodiesel) [12–14]. Therefore, in order to demonstrate the potential of these LS derived carbo-catalysts for industrial scale applications, continuous operations upon solketal production were conducted. Reactions were conducted over a fixed bed consisting of the most active LS catalyst, i.e. 80LS20PS450H$^+$ (details of reactor and catalyst bed preparation are given in the experimental section) under atmospheric pressure at varying temperatures and feed flow rate. In the current study, temperatures > 50 °C were avoided as to maintain the reaction mixture in liquid phase during operations. In first set of experiments, the influence of reaction temperature and acetone to glycerol molar ratio on the glycerol conversion was investigated. Fig. 9(a) summarizes the glycerol conversion from the various experiments conducted between 30 and 50 °C (solketal selectivity was > 99.5% in all cases), 1 atm and liquid flow rate of 0.1 ml/min, at acetone-to-glycerol equivalent ratio of 8:1 (anhydrous ethanol was used as solvent). The conversion trends observed were similar to the batch experiments and comparable at reaction temperatures 30 and 40 °C (90 ± 1), while the slightly reduced yield observed at 50 °C, was a consequence of backward equilibrium shifting (a typical feature of exothermic reactions). Meaning even the low reaction temperature of 30 °C was enough to drive the reaction towards completion and produced solketal in high yields (Fig. 9(a)) [19].

Fig. 9(b) shows the results of fixed bed experiments conducted at different reaction temperatures (30 and 50 °C) and at varying flow rates of reactant stream (0.05 ml/min, 0.1 ml/min and 0.2 ml/min) with the two feeds. At 50 °C, there was no visible effect of feed flow rate (0.05 ml/min and 0.1 ml/min) on glycerol conversion as the reaction proceeded at a faster rate (a short contact time was enough to drive the reaction to equilibrium). In contrast at 30 °C, where the reaction proceeded at a slower rate the positive effect of a low flow rate on solketal production could be clearly seen, with glycerol conversion reaching the lowest value (ca. 81 ± 1%) at 0.2 ml/min. In contrast, at 0.1 ml/min conversion 92 ± 1% could be reached. The trend observed here is in agreement with effect of increasing feed flow rate on reduced contact time/residence time. When the feed flow rate was increased to 0.2 ml/min, it is most likely that the reactants did not have sufficient time to interact efficiently inside the reaction zone, leading to the reduction of glycerol conversion [22–24]. The above data is consistent with the batch reaction data for 80LS20PS450H$^+$ (Fig. 8(b,c)) showing that the minimum time needed to reach equilibrium conversion is 15 min. Hence, 0.1 ml/min was selected as the optimum flow rate for further studies.

Also, as expected, an increase in the acetone-to-glycerol equivalent ratio from 6:1 to 8:1 resulted in a slight increase in the solketal production and is in agreement with the trends observed during the batch studies and literature [20,22,23]. In the current study, we opted for a excess of acetone (6 and 8) as (i) it reduces the viscosity of feed stream and reported to (ii) enhance catalyst lifetime by removing the H_2O by product formed during the reaction [20,23]. Use of a diluted glycerol stream (a high mole ratio of acetone/glycerol) has also been reported to be helpful for preventing reactor clogging as it reduces accumulation of unreacted substrate, solketal and H_2O on surface of catalyst particles [20,23].

Finally, the stability of 80LS20PS450H$^+$ catalyst was investigated over a longer time on stream (upto 90 h) using the two different feeds corresponding to acetone-to-glycerol mole ratio of 6:1 and 8:1 under the following experimental conditions: 50 °C, 0.1 ml/min and 1 atm. The trends observed and depicted in Fig. 10 show glycerol conversion as a function of time on stream confirm the exceptional stability of 80LS20PS450H$^+$ catalyst upon continuous solketal production. During the course of 90 h operations, the catalyst maintained its activity and selectivity, which could be attributed to its macro/mesoporous nature

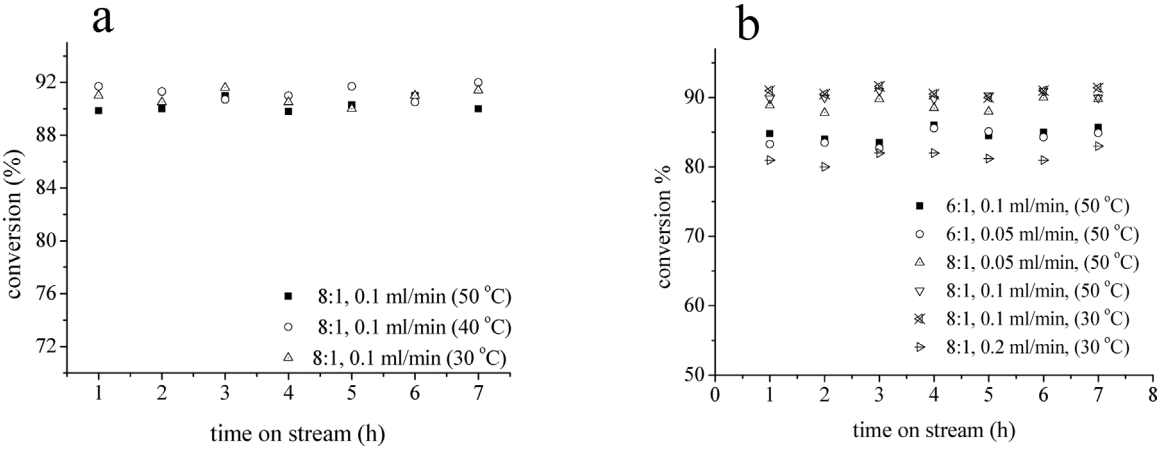

Fig. 9. Catalytic performance of 80LS20PS450H$^+$ catalyst in fixed bed operation as function of glycerol conversion vs. (a) reaction temperature at constant feed flow rate 0.1 ml/min and (b) effect of feed flow rate and acetone/glycerol (mole ratio); solketal selectivity was ≥99.5% in all cases.

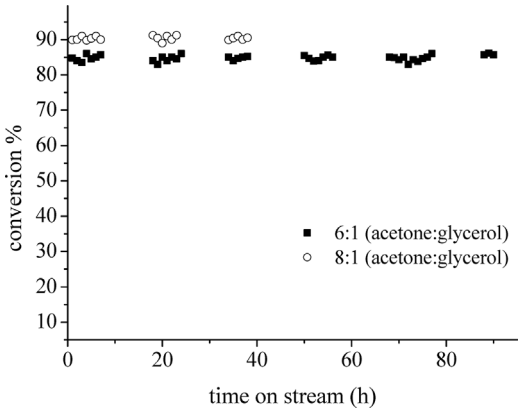

Fig. 10. Glycerol conversion over 80LS20PS450H$^+$ as function of time on stream at 50 °C and feed flow rate of 0.1 ml/min); solketal selectivity was ≥99.5% in all cases.

preventing blockage of active sites as well as its exceptionally stable active (−SO_3H) sites. The remarkable stability of the −SO_3H sites of 80LS20PS450H$^+$ was confirmed by FT-IR (Fig. S7, Supporting information) and XPS analysis, showing almost identical surface composition as fresh 80LS20PS450H$^+$ (Fig. 4(b)). Also, the catalyst could maintain its original pore structure as seen from the FE-SEM and TEM images (Figs. 6 and 7) and pore size distribution plots (Fig. S8, Supporting information). These results clearly indicate the superiority of LS based catalysts over previously reported sulfonic ion-exchange resin catalysts like Purolite®PD206, Amberlyst®15 and Amberlyst®36 showing deactivation within 8–24 h of operation [20,22–24].

4. Conclusions

Ice-templated LS or LS-PS monoliths were converted into strongly acidic macro/mesoporous solid protonic acids via mild pyrolysis and H^+ exchanging techniques avoiding the use of hazardous sulfonating agents. The resultant materials exhibited structural and textural characteristics similar to the well-known sulfonated carbons. Formation of porosity was favored at pyrolysis temperatures 400 °C and above; however, temperatures above 450 °C were found to have an adverse effect on the density of active/strong acid sites (−SO_3H density). Porosity development was also favored by partial substitution of LS by PS in the ice-templated monoliths. The resulting carbon materials demonstrated high activity as a solid Brønsted acid catalyst upon acetalization of glycerol with acetone, methyl levulinate and furfural (≥91% glycerol conversion). Moreover, the 80LS20PS450H$^+$ catalyst, due to its high porosity and stable −SO_3H sites showed exceptional activity (glycerol conversion up to 93%) and operational stability during liquid phase continuous flow solketal production (the catalyst retained its activity, structural and acidic features even after 90 h time on stream).

Acknowledgments

Kempe Foundations (Kempe stiftelserna), the Bio4Energy programme and Wallenberg Wood Science Center (WWSC) are gratefully acknowledged. Kempe Foundation is also acknowledged for providing postdoctoral fellowship to Lakhya Jyoti Konwar at Umeå University.

Appendix A. Supplementary data

Supplementary data associated with this article can be found, in the online version, at http://dx.doi.org/10.1016/j.apcatb.2017.08.061.

References

[1] J. Zakzeski, P.C. Bruijnincx, A.L. Jongerius, B.M. Weckhuysen, Chem. Rev. 110 (2010) 3552–3599.
[2] E. Mikkola, A.W.T. King, P. Virtanen, The biorefinery and green chemistry, in: R.B. Lukasik (Ed.), Ionic Liquids in the Biorefinery Concept: Challenges and Perspectives, RSC Green Chemistry, 2015, pp. 1–37 Book series.
[3] R. Ma, Y. Xu, X. Zhang, ChemSusChem 8 (2015) 24–51.
[4] S.E. Lebo Jr., J.D. Gargulak, D. Jerry, T.J. McNally, Lignin, Kirk-Othmer Encyclopedia of Chemical Technology, John Wiley & Sons, Inc., 2001.
[5] W. Chen, X. Peng, L. Zhong, Y. Li, R. Sun, ACS Sustain. Chem. Eng. 3 (2015) 1366–1373.
[6] H. Xie, Z.K. Zhao, Q. Wang, ChemSusChem 5 (2012) 901–905.
[7] S. Li, N. Li, G. Li, L. Li, A. Wang, Y. Cong, X. Wang, T. Zhang, Green Chem. 17 (2015) 3644–3652.
[8] X. Zhang, Z. Zhang, F. Wang, Y. Wang, Q. Song, J. Xu, J. Mol. Catal. A: Chem. 377 (2013) 102–107.
[9] D. Lee, Molecules 18 (7) (2013) 8168–8180.
[10] A. Casas, J.R. Ruiz, M.J. Ramos, A. Perez, Energy Fuels 24 (2010) 4481–4489.
[11] L.J. Konwar, P. Mäki-Arvela, P. Begum, N. Kumar, A.J. Thakur, J.-P. Mikkola, R.C. Deka, D. Deka, J. Catal. 329 (2015) 237–247.
[12] S. Nicolas, F. Grigoletto, S. Martins, (2017) WO2017006141.
[13] C.J.A. Mota, C.X.A. da Silva, N. Rosenbach Jr., J. Costa, F. da Silva, Energy Fuels 24 (2010) 2733–2736.
[14] E. García, M. Laca, E. Pérez, A. Garrido, J. Peinado, Energy Fuels 22 (6) (2008) 4274–4280.
[15] H. Serafima, I.M. Fonsecab, A.M. Ramosb, J. Vitalb, J.E. Castanheiro, Chem. Eng. J. 178 (2011) 291–296.
[16] P.S. Reddy, P. Sudarsanam, B. Mallesham, G. Raju, B.M. Reddy, J. Ind. Eng. Chem. 17 (3) (2011) 377–381.
[17] B. Mallesham, P. Sudarsanam, G. Rajua, B.M. Reddy, Green Chem. 15 (2013) 478–489.
[18] P. Ferreiraa, I.M. Fonsecab, A.M. Ramosb, J. Vitalb, J.E. Castanheiro, Appl. Catal. B: Environ. 98 (1–2) (2010) 94–99.
[19] M.R. Nanda, Z. Yuan, W. Qin, H.S. Ghaziaskar, M.-A. Poirier, C.C. Xu, Fuel 117 (2014) 470–477.
[20] P.A. Oliveira, R.O.M.A. Souza, C.J.A. Mota, J. Braz. Chem. Soc. 27 (10) (2016) 1832–1837.
[21] D. Nandan, P. Sreenivasulu, L.N.S. Konathala, M. Kumar, N. Viswanadham, Microporous Mesoporous Mater. 179 (15) (2013) 182–190.
[22] M.R. Nanda, Z. Yuan, W. Qin, H.S. Ghaziaskar, M.-A. Poirier, C.C. Xu, Appl. Energy 123 (2014) 75–81.
[23] M. Shirani, H.S. Ghaziaskar, C.C. Xu, Fuel Process. Technol. 124 (2014) 206–211.
[24] Y.M. Gorji, H.S. Ghaziaskar, Ind. Eng. Chem. Res. 55 (2016) 6904–6910.
[25] H. Zhang, A.I. Cooper, Adv. Mater. 19 (2007) 1529–1533.
[26] M. Kitano, K. Arai, A. Kodama, T. Kousaka, K. Nakajima, S. Hayashi, M. Hara, Catal Lett. 131 (2009) 242.
[27] X. Mo, D.E. López, K. Suwannakarn, Y. Liu, E. Lotero, J.G. Goodwin Jr., J. Catal. 254 (2) (2008) 332–338.
[28] L.J. Konwar, R. Das, A.J. Thakur, E. Salminen, P. Mäki-Arvela, N. Kumar, J.-P. Mikkola, D. Deka, J. Mol. Catal. A Chem. 388–389 (2014) 167–176.
[29] Y.S. Kim, S.J. Yang, H.J. Lim, T. Kim, C.R. Park, Carbon 50 (2012) 3315–3323.
[30] A.D. Roberts, X. Li, H. Zhang, Carbon 95 (2015) 268–278.
[31] M. Hara, T. Yoshida, A. Takagaki, T. Takata, J.N. Kondo, S. Hayashi, K. Domen, Angew. Chem. Int. Ed. 43 (22) (2004) 2955–2958.
[32] H. Marsh, P.M.A. Sherwood, D. Augustyn, Fuel 55 (2) (1976) 97–98.
[33] X. Li, S.P. Lau, L. Tang, R. Ji, P. Yang, Nanoscale 6 (2014) 5323–5328.
[34] L.J. Konwar, P. Mäki-Arvela, E. Salminen, N. Kumar, A.J. Thakur, J.-P. Mikkola, D. Deka, Appl. Catal. B Environ. 176–177 (2015) 20–35.
[35] B.L. Wegenhart, S. Liu, M. Thom, D. Stanley, M.M. Abu-Omar, ACS Catal. 2 (12) (2012) 2524–2530.
[36] C. Gonzalez-Arellano, R.A.D. Aranconb, R. Luque, Green Chem. 16 (2014) 4985–4993.
[37] B. Bruchmann, K. Haberle, H. Gruner, M. Hirn, (1999) US 5917059A.
[38] S. Selifonov, (2014) US8906961 B2.